21st Australasian Fluid Mechanics Conference
Adelaide, Australia
10-13 December 2018

Fluid Flow and Heat Transfer of Gas-Liquid Two-Phase Flow in Microchannels

Ayoub Abdollahi, S.E. Norris and Rajnish N. Sharma

Department of Mechanical Engineering, University of Auckland, Auckland 1142, New Zealand

Abstract

The fluid flow and heat transfer behavior of gas-liquid two-phase flows in square and rectangular microchannels is studied using a three-dimensional numerical simulation. The liquid film thickness, friction factor and heat transfer rate of the gas-liquid Taylor flow are investigated in detail using a volume of fluid method (VOF). The performance evaluation criterion (*PEC*) was used to compare the performance of using two-phase Taylor flow against a single-phase flow. The interface in the cross-section of the gas bubble has a saddle shape, resulting in a non-uniform film thickness at the wall. An enhancement in the rate of heat transfer was seen for increasing Reynolds number, decreasing gas volume fraction and decreasing slug length.

Introduction

Dissipating a high heat flux is an important issue of modern thermal management with the ever-increasing demands for high performance and miniaturization [1]. According to the literature [2] traditional electronic cooling systems are no longer efficient enough to meet the needs of electronic systems. The magnitude of generated heat flux in computer technology is projected to increase from 300 W/cm^2 to 500 W/cm^2 and 1000 W/cm^2 at hot spots, or even higher in some cases [15]. As a result there has been an interest in the use of microchannel heat sinks (MCHS) as devices for the removal of heat from microelectronic systems.

The concept of the MCHS is defined as small mass and volume devices with high convective heat transfer coefficients and large surface area to volume ratio. They were first proposed in 1982 by Tuckerman and Pease [3]. By using MCHS, the heat transfer coefficient could be enhanced by periodic interruption of the thermal boundary layer, better flow mixing and increasing turbulence intensity through the generation of secondary flow.

Water is the most desirable coolant used in a MCHS. However, heat transfer of two-phase flow in microchannels is significantly higher than with a single phase flow [1, 4]. Recent studies [5, 6] have considered replacing the single liquid based flow system with a gas liquid two-phase flow system. In such a Taylor bubble two-phase flow system without phase change, bubbles are periodically arranged in a carrier liquid in the microchannel, leading to a significant increase in the heat transfer rate.

Numerical models of Taylor bubbles in microchannels have used either a fixed frame of reference (FFR) or a moving frame (MFR). Santos and Kawaji [7], Qian and Lawal [8], and Shao et al. [9] used FFR methods in their studies, while Araújo et al. [10], Asadolahi et al. [11, 12] , Dai et al. [6] and Zhang et al. [13] used MFR methods. For a 3D simulation a MFR method is preferable to reduce computational time. A more detailed description of these mentioned methods can be found in Asadolahi et al.[12].

A survey of the literature suggests that simulations of Taylor bubble flow have been limited to 2D, and there is a lack of an in-depth study to investigate the heat transfer of Taylor two-phase flow in rectangular microchannels [14]. This has motivated the authors' present work. The current study examines 3D gas-liquid Taylor flow of Air/water in a square and rectangular microchannel. The film thickness, Nusselt number, friction factor and performance evaluation criterion (*PEC*) are reported and compared with results using single phase liquid water as the working fluid.

Numerical Model

The numerical simulation of two-phase Taylor flow is performed by solving the governing equations (continuity, momentum, and energy equations) using a volume of fluid (VOF) method with a propriety computational fluid dynamics (CFD) software package (ANSYS Fluent, Release 17.0). A double precision transient solver is used in this study. The two phases are assumed incompressible and do not penetrate or mix with each other. The interface of the two phases is modelled by solving an additional advection equation for the volume fraction. The surface tension can be calculated by the continuum surface force (CSF) model introduced by Brackbill et al. [15].

Five parameters including the Reynolds number Re, Capillary number Ca, film thickness δ, friction factor f, Nusselt number Nu and the Performance evaluation criterion PEC [20] are considered in the present work. All the parameters are calculated based on the properties of the liquid phase. The parameters are defined as:

$$Re = \rho u_{TP} D_h / \mu \quad (1)$$

$$Ca = \mu u_{TP} / \sigma \quad (2)$$

$$f = \Delta p D_h / 2 L_{Slug} \rho (u_{TP})^2 \quad (3)$$

$$Nu = q D_h / A[T_{w,ave} - T_{f,ave}] \quad (4)$$

$$PEC = \mathrm{Nu}/\mathrm{Nu}_o \ / \ (f/f_o)^{1/3} \quad (5)$$

Numerical Method

The moving domain method (dynamic mesh method in Fluent) was used to simulate the fully developed fluid flow and heat transfer of two-phase flow with constant heat flux on the walls. A Poiseuille flow velocity profile was used for initial conditions.

A rectangular bubble with a prescribed volume is initialised into the centre of the computational domain. An isothermal flow field is initially solved to steady state. The energy equation is then solved on this flow field. A periodic boundary condition for temperature is applied using equation (6) as recommended by Asadolahi et al. [12].

$$\Delta T_{UC} = \frac{4qL}{D\left[\epsilon v_B \rho_G C_{cG} + \left(v_{tp} - \epsilon v_B\right)\rho_L C_{pL}\right]} \quad (6)$$

Boundary Conditions

The inlet boundary is specified as a velocity-inlet. The downstream boundary is assigned a pressure-outlet with an average pressure of zero. The walls are no-slip with a constant heat flux (30,000 w/m^2). User defined functions (UDFs) are used to calculate the bubble velocity and to apply the periodic boundary conditions for temperature and velocity.

Solver Options

The Green-Gauss node-based method was used, with the implicit body force method for body forces. The QUICK scheme was applied to discretise the momentum and energy equations. Pressure and volume fraction were discretized by the body-force weighted and Geo-Reconstruct interpolation schemes respectively. The Non-Iterative Time-Advancement Scheme with a variable time step based on a Courant number of 0.25 was used for the time marching of the continuity and, momentum equations. However, the energy equation was solved using a constant time-step of 10^{-4} s.

Grid testing

A unit-cell including one bubble and two halves of liquid slug was considered as the computational domain with width and depth of 1mm.The Grid Convergence Index (GCI) method, based on Richardson extrapolation, was used to estimate the mesh dependency and discretisation error for the simulations. Three meshes (coarse, medium and fine) with 216,000, 512,000 and 1,124,000 elements were used to determine a suitable grid size. The bubble length, friction factor (*f)* and Nusselt numbers (*Nu)* for the three meshes are reported in Table 1. It was found that changing the mesh resolution from medium to fine only reduced the maximum error by approximately 3 %. Hence, in order to reduce the computation time, the medium mesh, with a minimum of 10 elements in the film region, was selected.

	Axial Bubble Length (mm)	*f*	*Nu*
GCI_{fine}^{21}(%)	0.36	0.52	3.30

Table 1 Discretization error

Results and discussion

Variation of Bubble Shapes and Bubble length

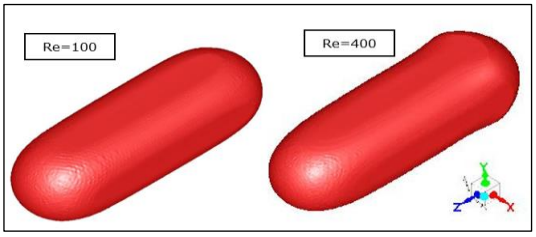

Figure 1. Bubble shape for *Re*=100 and *Re* =400 with constant bubble volume.

The bubble shapes for two different Reynolds numbers for the same void fraction are presented in figure 1. The interface close to the wall is flat due to the confining effect from the microchannel wall. Confining the bubble in the radial direction leads to an increase in the bubble length in the axial direction. At the ends of the bubble, the interface becomes hemispherical due to the dominant influence of surface tension at microscale. It can be seen that by increasing the Reynolds number from 100 to 400, the bubble shape is deformed to a bullet shape. This was due to a pressure change in the liquid film region along the bubble. Figure 2 shows that the bubble length increases with increasing the Reynolds number. Asadolahi et al. [12] experimentally obtained similar results for a circular tube.

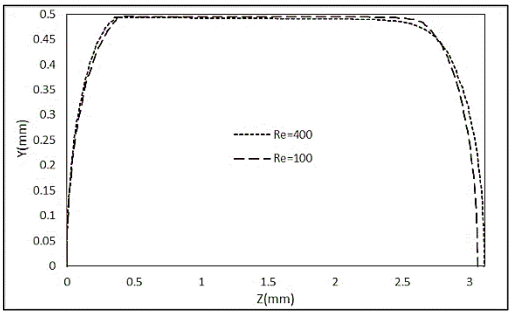

Figure 2. Bubble interface on microchannel centre-plane for Re=100 and Re=400, for constant bubble volume

Liquid Film Thickness

The shape of the bubble and the film thickness depend on the geometry, the liquid properties, and the flow conditions [16]. Thus, the Capillary number *Ca* is used to parameterise the film thickness. The capillary number represents the ratio between viscous and surface tension forces between the two liquid phases. Figure 3 presents the corner film thickness, as defined in figure 4, for varying *Ca*. The film thickness at the corner δ_{corner} is increased by increasing *Ca* from 0.001 to 0.0077. The results are in a good agreement with Eq. 7 from Han and Shikazono [21], with a maximum error of 5 percent.

$$\frac{2\delta_{corner}}{D_h} = \frac{2.43\ Ca^{2/3}}{1 + 7.28Ca^{2/3} - 0.255\ We^{0.215}} - 0.243 \qquad (7)$$

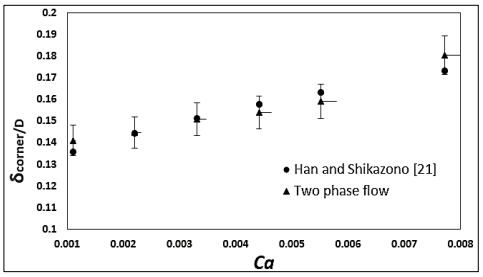

Figure 3. Film thickness at the corner.

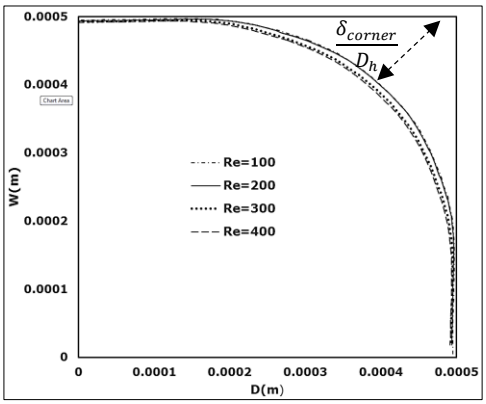

Figure 4. Bubble interface at the cross-section of the microchannel.

Figure 4 shows the predicted gas-water interface at the section where the film thickness becomes constant, for different *Re*. The bubble shape in the rectangular geometry differs from that in a circular tube. At low *Ca*, the confining effect makes the bubble naturally asymmetric, and the liquid film is thicker at the corner compared to the liquid film on the sides. The liquid film thickness at the side is not constant, and the interface has a saddle shape as shown in figure 4. The film thickness at the corner increases by increasing the *Ca*, while there is a slight change in the film thickness at the sides.

Friction Factor and Heat Transfer

Effect of Re

The frictional characteristics of laminar single-phase, and gas-liquid Taylor flow, versus Reynolds number for a bubble with the volume fraction of 0.3 is presented in figure 5-a. The two-phase flow has a higher friction factor than single phase flow. This is due to the presence of the gas bubble causing secondary flows, which increases the frictional dissipation in the flow. As with single phase flow, the friction factor decreases with increasing *Re*. Kreutzer et al. [17]proposed the correlation (Eq. 8) to predict the friction factor of Taylor bubble flow in a circular microchannel. Figure 5-a shows that Eq. 8 can be used to predict the friction factor of gas-liquid Taylor flow in the square microchannel for *Re* over 200 with an error less than 10%. Higher errors ranging from 10 % to 20 % are seen for *Re* less than 200.

$$f = \frac{16}{Re}\left[1 + 0.07\frac{D_h}{L_{Slug}}\left(\frac{R}{Ca}\right)^{\frac{1}{3}}\right] \quad (8)$$

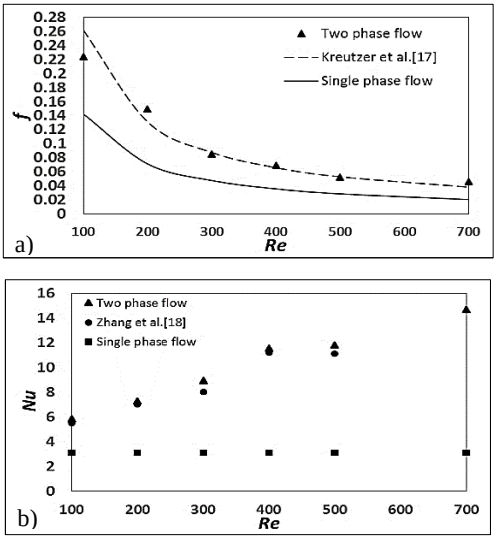

Figure 5. a) Friction factor and b) Nusselt number as functions of *Re*.

Figure 5-b represents the Nusselt number (*Nu*) for varying Reynolds number. For a constant bubble volume fraction, increasing the velocity of two-phase flow increases the *Nu*, unlike single phase flow for which it is constant. Increasing the *Re* increases the advection heat transfer causing the increase in *Nu*. The present results agree well with those of Zhang et al.[18].

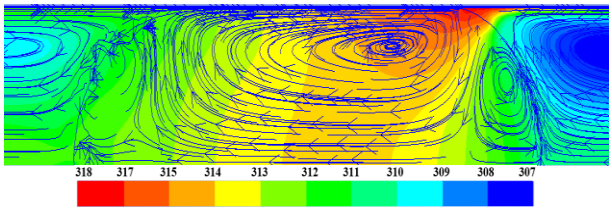

Figure 6. Temperature profile

Figure 6 shows a temperature contour plot and velocity vector in both the phases. The recirculation in the primary phase (water) results in a higher temperature variation in the slug region by moving the hot fluid close to the wall to the centre of the channel. The gas bubble has a higher temperature due to its low heat capacity. The rear of the bubble has the highest temperature since the fluid inside the bubble moves along opposite directions close to the wall, gaining energy (heat) from the wall. In addition, there is a heat transfer between bubble and slug region.

Effect of the Gas Volume Fraction

The Nusselt number and friction factor for a constant *Re* versus secondary phase volume fraction are presented in figure 7a-b. The friction factor increases and *Nu* number decreases with an increase in the gas volume fraction (ϵ). As shown in figure 6, a small temperature variation occurs in the secondary phase due to its low involvement in the total heat transfer. Thus increasing the bubble volume in a unit-cell decreases the *Nu*.

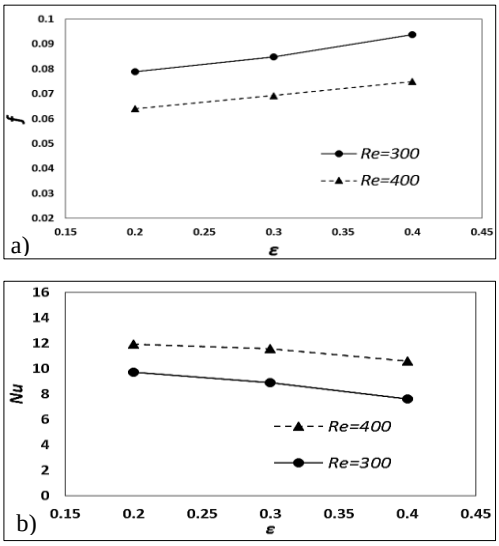

Figure 7. Effect of ϵ on a) Friction factor, b) *Nu*.

Effect of Unit-cell Length

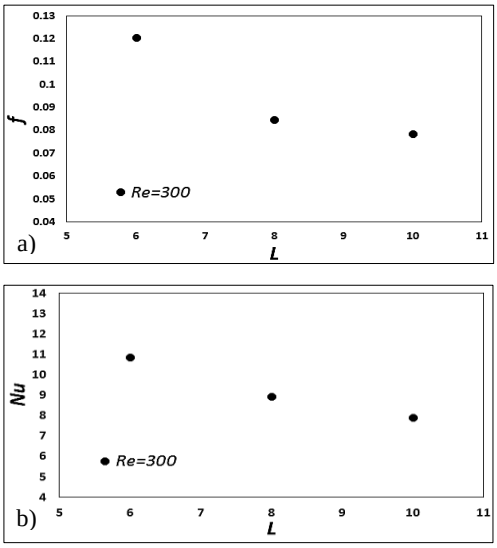

Figure 8. a) Friction factor, and b) Nusselt number

Figure 8 shows the results obtained for three different unit-cell lengths (*L*), for a constant ϵ of 30%. Figure 8 indicates that increasing the slug length decreases the *Nu* and friction factor. By increasing slug length the effect of Laplace pressure drop decreases, causing a lower friction factor for the longer unit-cell. The Taylor bubble does not contribute to the heat transfer due to lower thermal conductivity of the gas compared to that of water. By increasing the slug length, the Nusselt number has a tendency to reduce to that of fully developed single phase laminar flow. A shorter slug length results in a stronger internal recirculation resulting in a higher heat transfer rate. This phenomenon was reported for circular micro-tubes by Dai et al. [7].

Performance Evaluation Criteria (*PEC*)

The *PEC* is used as the criterion to compare the performance of each configuration. As shown in figure 9, the two-phase Taylor bubble enhances the microchannel performance. Besides, the *PEC* decreases with increasing ϵ as the friction factor increases and *Nu* number is decreased. Although increasing the slug length decreses the performance of the channel but the *PEC* value is still higher than one indicating the importance of the recirculation happening in the slug region.

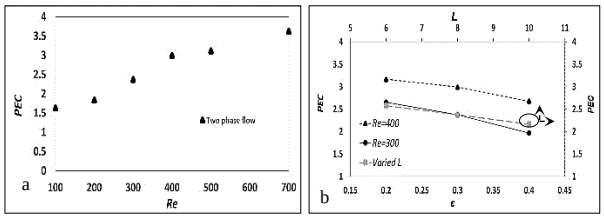

Figure 9 *PEC*, a) constant ϵ, b) varied ϵ and varied *L* with constant ϵ

Heat Transfer Prediction

Leung et al.[19] presented Eq.9 to calculate heat transfer of Taylor flow in a vertical circular tube.

$$Nu_l^* = 4.364 + 0.13\left(L_{slug}^*\right)^{-0.46} Ca^{-0.30} \qquad (9)$$

where $L_{slug}^* = \frac{L_{slug}}{Re\ Pr\ D_h}$.

A correlation was obtained based on the numerical data obtained in the present study, to predict *Nu* in the microchannel with square and rectangular cross-section with a varied aspect ratio (1< *AR* <*2*) using Eq.9. The maximum deviation is 12 % for *Re*=100.

$$Nu_{TP} = (3.091 + 0.053\mathrm{AR}^{0.137}\left(L_{slug}^*\right)^{-0.772} Ca^{-0.094})\ (1-\epsilon) \qquad (10)$$

Conclusions

Three-dimensional numerical simulations were used to study the fluid flow and heat transfer of gas-liquid two-phase flows in a square and rectangular microchannel. The friction factor decreased with increasing *Re*, decreasing gas volume fraction and increasing the unit-cell length. The cross section of the gas-liquid interface of the bubble has a saddle shape, resulting in a non-uniform film thickness. *Nu* increased for increasing *Re*, decreasing gas volume fraction and decreasing slug length. An enhancement in the performance over single phase flow (*PEC*) ranging from 1.5 to 3.5 was seen by using gas-liquid Taylor flow.

References

[1] Smakulski, P. and Pietrowicz, S., A review of the capabilities of high heat flux removal by porous materials, microchannels and spray cooling techniques, *Applied Thermal Engineering*, **104**, 636-646, 2016.

[2] Chai, L., Xia, G., Zhou, M., Li, J. and Qi, J., Optimum thermal design of interrupted microchannel heat sink with rectangular ribs in the transverse microchambers, *Applied Thermal Engineering*, **51**, 880-889, 2013.

[3] Tuckerman, D.B. and Pease, R.F.W., High-Performance Heat Sinking for VLSI, *IEEE Electron Device Letters*, **EDL-2**, 126-129, 1981.

[4] Qu, W. and Mudawar, I., Prediction and measurement of incipient boiling heat flux in micro-channel heat sinks, *International Journal of Heat and Mass Transfer*, **45**, 3933-3945, 2002.

[5] Bandara, T., Cheung, S.C.P. and Rosengarten, G., Slug flow heat transfer in microchannels: a numberical study, **7**, 81-92, 2015.

[6] Dai, Z., Guo, Z., Fletcher, D.F. and Haynes, B.S., Taylor flow heat transfer in microchannels—Unification of liquid–liquid and gas–liquid results, *Chemical Engineering Science*, **138**, 140-152, 2015.

[7] Santos, R.M. and Kawaji, M., Numerical modeling and experimental investigation of gas-liquid slug formation in a microchannel T-junction, *International Journal of Multiphase Flow*, **36**, 314-323, 2010.

[8] Qian, D. and Lawal, A., Numerical study on gas and liquid slugs for Taylor flow in a T-junction microchannel, *Chemical Engineering Science*, **61**, 7609-7625, 2006.

[9] Shao, N., Salman, W., Gavriilidis, A. and Angeli, P., CFD simulations of the effect of inlet conditions on Taylor flow formation, *International Journal of Heat and Fluid Flow*, **29**, 1603-1611, 2008.

[10] Araújo, J.D.P., Miranda, J.M., Pinto, A.M.F.R. and Campos, J.B.L.M., Wide-ranging survey on the laminar flow of individual Taylor bubbles rising through stagnant Newtonian liquids, *International Journal of Multiphase Flow*, **43**, 131-148, 2012.

[11] Asadolahi, A.N., Gupta, R., Leung, S.S.Y., Fletcher, D.F. and Haynes, B.S., Validation of a CFD model of Taylor flow hydrodynamics and heat transfer, *Chemical Engineering Science*, **69**, 541-552, 2012.

[12] Asadolahi, A.N., Gupta, R., Fletcher, D.F. and Haynes, B.S., CFD approaches for the simulation of hydrodynamics and heat transfer in Taylor flow, *Chemical Engineering Science*, **66**, 5575-5584, 2011.

[13] Zhang, J. and Li, W., Investigation of hydrodynamic and heat transfer characteristics of gas–liquid Taylor flow in vertical capillaries, *International Communications in Heat and Mass Transfer*, **74**, 1-10, 2016.

[14] Abdollahi, A., Sharma, R.N. and Vatani, A., Fluid flow and heat transfer of liquid-liquid two phase flow in microchannels: A review, *International Communications in Heat and Mass Transfer*, **84**, 66-74, 2017.

[15] Brackbill, J.U., Kothe, D.B. and Zemach, C., A continuum method for modeling surface tension, *Journal of Computational Physics*, **100**, 335-354, 1992.

[16] Che, Z., Wong, T.N., Nguyen, N.-T. and Yang, C., Three dimensional features of convective heat transfer in droplet-based microchannel heat sinks, *International Journal of Heat and Mass Transfer*, **86**, 455-464, 2015.

[17] Kreutzer, M.T., Kapteijn, F., Moulijn, J.A., Kleijn, C.R. and Heiszwolf, J.J., Inertial and interfacial effects on pressure drop of Taylor flow in capillaries, *AIChE Journal*, **51**, 2428-2440, 2005.

[18] Zhang, J., Fletcher, D.F. and Li, W., Heat transfer and pressure drop characteristics of gas–liquid Taylor flow in mini ducts of square and rectangular cross-sections, *International Journal of Heat and Mass Transfer*, **103**, 45-56, 2016.

[19] Leung, S.S.Y., Gupta, R., Fletcher, D.F. and Haynes, B.S., Effect of flow characteristics on Taylor flow heat transfer, *Industrial and Engineering Chemistry Research*, **51**, 2010-2020, 2012.

[20] Abdollahi, A., Sharma, R.N., Mohammed, H.A. and Vatani, A., Heat transfer and flow analysis of Al2O3-Water nanofluids in interrupted microchannel heat sink with ellipse and diamond ribs in the transverse microchambers, *Heat Transfer Engineering*,1-9, 2017.

[21] Han, Y. and Shikazono, N., Measurement of liquid film thickness in micro square channel, *International Journal of Multiphase Flow*, **35**, 896-903, 2009.